Computational Modeling of Tip Heat Transfer to a Superscale Model of an Unshrouded Gas Turbine Blade

Brian M. T. Tang
e-mail: brian.tang@eng.ox.ac.uk

Pepe Palafox[1]

Department of Engineering Science,
University of Oxford,
Parks Road,
Oxford OX1 3PJ, UK

Brian C. Y. Cheong
Rolls-Royce plc.,
Turbine Systems (FH-3),
Bristol BS34 7QE, UK
e-mail: brian.cheong@rolls-royce.com

Martin L. G. Oldfield
e-mail: martin.oldfield@eng.ox.ac.uk

David R. H. Gillespie
e-mail: david.gillespie@eng.ox.ac.uk

Department of Engineering Science,
University of Oxford,
Parks Road,
Oxford OX1 3PJ, UK

Control of over-tip leakage flow between turbine blade tips and the stationary shroud is one of the major challenges facing gas turbine designers today. The flow imposes large thermal loads on unshrouded high pressure (HP) turbine blades and is significantly detrimental to turbine blade life. This paper presents results from a computational study performed to investigate the detailed blade tip heat transfer on a sharp-edged, flat tip HP turbine blade. The tip gap is engine representative at 1.5% of the blade chord. Nusselt number distributions on the blade tip surface have been obtained from steady flow simulations and are compared with experimental data carried out in a superscale cascade, which allows detailed flow and heat transfer measurements in stationary and engine representative conditions. Fully structured, multiblock hexahedral meshes were used in the simulations performed in the commercial solver FLUENT. Seven industry-standard turbulence models and a number of different tip gridding strategies are compared, varying in complexity from the one-equation Spalart–Allmaras model to a seven-equation Reynolds stress model. Of the turbulence models examined, the standard k-ω model gave the closest agreement to the experimental data. The discrepancy in Nusselt number observed was just 5%. However, the size of the separation on the pressure side rim was underpredicted, causing the position of reattachment to occur too close to the edge. Other turbulence models tested typically underpredicted Nusselt numbers by around 35%, although locating the position of peak heat flux correctly. The effect of the blade to casing motion was also simulated successfully, qualitatively producing the same changes in secondary flow features as were previously observed experimentally, with associated changes in heat transfer with the blade tip. [DOI: 10.1115/1.3153307]

1 Introduction

The pursuit of increased performance in modern gas turbine design has driven turbine entry temperatures steadily toward the stoichiometric combustion temperature, subjecting turbine blade tips to an increasingly harsh environment. Modern engines running at higher speeds impose increased mechanical loads both on the shroud of a shrouded HP turbine blade and the structure required to support it. In spite of the additional tip leakage expected, there has, therefore, been a gradual shift toward unshrouded alternatives. This has brought tip heat transfer and leakage flow to the forefront and made it a priority for aeroengine research.

A review of tip leakage research was presented in 2001 by Bunker [1], which details many experimental and some computational investigations of the subject. Mayle and Metzger [2] presented the first blade tip heat transfer study, performed using a simple 2D model representative of a blade tip. A rotating cylinder suspended above the test surface simulated the moving endwall. In doing so, the authors found the effect of the relative endwall motion to be minimal, a conclusion that has not always been supported by more recent studies undertaken in cascade environments. Yaras and Sjolander [3] investigated the effect of relative endwall motion in an aerodynamic study performed in a linear cascade using an electrically driven rubber belt as the endwall. A relatively large tip gap of 3.8% chord was used, allowing a low-blockage three hole probe to measure the leakage flow directly. A 50% leakage mass flow reduction was observed when the belt was run at an engine representative speed.

Azad et al. [4,5] used a transient liquid crystal technique on a linear cascade using the GE-E^3 first rotor stage aerofoil to study the heat transfer to the blade tip surfaces of both flat tip and squealer tip blades. Heat transfer measurements in both cases were taken at tip clearances of 1%, 1.5%, and 2.5% blade spans. The squealer tips showed significantly reduced heat transfer compared with the flat tips at similar tip conditions. The magnitude of measured heat transfer for both geometries was found to be very sensitive to tip clearance, although the spatial distributions were qualitatively unchanged by the tip gap. Further squealer tip configurations were later tested by Kwak et al. [6] using the same cascade.

As the price of computational power has fallen, numerical investigations into the tip flow have become ever more popular. Bunker et al. [7] presented the experimental data obtained using a similar technique to that employed by Azad et al. [4,5] with a two-passage linear cascade. Ameri and Bunker [8] simulated the experimental rig numerically, using hexahedral meshes run with the LERC-HT solver and the Wilcox k-ω turbulence model [9] with modifications by Menter [10]. A sharp-edged flat tip was simulated as well as a radiused-edged flat tip. The agreement between the experimentally measured and computationally predicted heat transfer coefficients was reasonably good over the majority of the tip surface, with a typical discrepancy of 15–20% in heat transfer coefficient for the sharp-edged blade. The prediction of the radiused-edged blade was better, with errors below 15% over the tip surface due to the elimination of the separation and reattachment on the pressure side edge. Yang et al. [11,12] simulated the

[1]Present address: GE Corporate Research, Schnectady, NY 12309.

Contributed by the International Gas Turbine Institute of ASME for publication in the JOURNAL OF TURBOMACHINERY. Manuscript received March 2, 2009; final manuscript received March 16, 2009; published online April 7, 2010. Review conducted by David Wisler. Paper presented at the ASME Turbo Expo 2008: Land, Sea and Air (GT2008), Berlin, Germany, June 9–13, 2008.

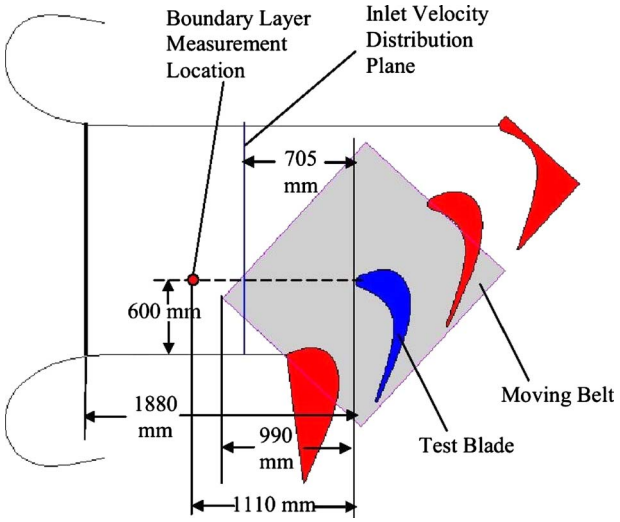

Fig. 1 Schematic of the linear cascade

GE-E^3 blade used by Azad et al. [4,5] with unstructured meshes solved in FLUENT. They simulated a single blade with the use of periodic boundary conditions and compared their heat transfer predictions to those measured by Azad et al. [4,5], achieving reasonable agreement with both the flat tip and the squealer tip blades. Three turbulence models were used in each case: the standard k-ε model, renormalized grouping (RNG) k-ε model, and Reynolds stress model (RSM). In both cases, the standard k-ε model was found to overpredict the heat transfer coefficient, while the RNG k-ε model was the best for the flat tip and the RSM proved the best for the squealer tip. The overprediction found with the standard k-ε model was attributed to excessive production of turbulent kinetic energy in the shear layer around the separation bubble on the pressure side edge.

In this paper, a test of seven different turbulence models is performed on large scale blades at engine representative speeds. The predicted heat transfer coefficient distributions are compared with the experimental data obtained from the Oxford superscale cascade [13,14]. The effect of a moving endwall on the heat transfer distribution to the blade tip is also simulated.

2 Experimental Setup

Details of the experimental setup in the Oxford superscale cascade and the experimental conditions used are fully described in Refs. [13–15], and are described briefly here for completeness. A three-passage linear cascade was used, with a motorized rubber belt to allow the moving endwall to be simulated, as shown in Fig. 1. The belt extends far enough upstream to ensure a correctly skewed boundary layer at the blade leading edge. The blade profile used is a low speed version of the RT27a aerofoil, a high-work HP turbine blade somewhat representative of those found in modern aeroengines. The blades have a chord of 1 m, an axial chord of 0.808 m, a span of 1 m, and turn the flow through 111.45 deg. All of the edges on the blade tip are sharp. All simulations were performed at a tip gap of 15 mm (1.5% chord). The cascade Reynolds number, based on axial chord and cascade exit conditions, was 4.0×10^5, with a freestream velocity of 3.5 m/s and a cascade exit velocity of 7 m/s. The experimental conditions are summarized in Table 1.

Blade tip surface temperature measurements were made using infrared thermography in steady-state experiments, as fully reported in Refs. [13,15]. For this experiment, the flat tip of the instrumented blade was constructed from a laminated sandwich of glue, Kapton, and copper as shown in Fig. 2. The copper layer was photochemically machined to create a series of 5 mm wide rectangular copper strips with 0.5 mm gaps between neighboring

Table 1 Summary of experimental conditions

True chord	1.0 m
Axial chord	0.808 m
Blade span	1.0 m
Blade turning angle	111.45 deg
Tip gap	15 mm
Reynolds number	4.0×10^5
Freestream velocity	3.5 m s^{-1}
Cascade exit velocity	7 m s^{-1}

strips. A current passed in series through these strips produced a constant heat flux condition. The input DC current and voltage were monitored throughout the experiment. Steady-state conditions were obtained after 10–15 min of operation. The temperature of the back surface of the tip, which was painted black to provide a surface of known emissivity, was monitored using an IR camera. The temperature resolution of the camera was $<0.15\,^\circ$C, while the spatial resolution was 320×240 pixels. To obtain sufficient resolution, images were recorded at three camera positions and a composite image was used in subsequent analysis. Three foil thermocouples mounted on the test surface provided reference temperatures to aid data processing and real-time IR camera calibration, while also providing reference locations to allow the images to be accurately aligned. These measurements, combined with an upstream air temperature measurement by a thermocouple, allowed heat transfer data to be determined. Corrections were made for radiation by considering the inside of the blade cavity as a black body and the tip gap as a pair of parallel plates of known emissivity. Furthermore, free convection in the blade cavity and lateral conduction losses in the tip substrate were corrected for, making the final equation used to compute the convective heat transfer coefficient

$$h=\frac{\dfrac{VI-RI^2}{A_s}-\epsilon\sigma(T_w^4-T_g^4)}{T_w-T_g}-0.4717(T_w-T_g)^{0.5339} \quad (1)$$

This measurement and calculation has an associated typical uncertainty in heat transfer coefficient of 5%, rising to 16% for peak values in heat transfer coefficient [13], as shown in Table 2, calculated using a perturbation technique [16]. The measures and associated uncertainty are detailed in Table 2. All heat transfer results are presented in the form of Nusselt number, nondimensionalized with respect to the blade axial chord (0.808 m). Flow velocity measurements were also obtained by particle image velocimetry and are fully reported in Refs. [13,14].

2.1 Computational Method. The simulations described in the present study were performed in the unstructured commercial solver FLUENT 6.3. The pressure-based implicit solver, a cell-

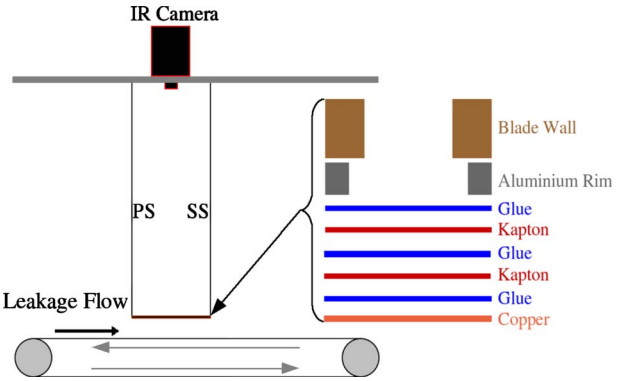

Fig. 2 Layers comprising the 210 μm thick blade tip

Table 2 Uncertainty analysis results for minimum, maximum, and typical values of *h*

Parameter		Typical values for min/max/typical h	δX_i	$\frac{\partial h}{\partial X_i}\delta X_i$
V	Min	27.68		0.1004
	Max	27.44	0.138	0.6782
	Typical	27.6		0.2950
I	Min	4.5		0.1004
	Max	4.5	0.023	0.6782
	Typical	4.5		0.2950
R	Min	0.3418		−0.0112
	Max	0.3418	0.003418	−0.0760
	Typical	0.3418		−0.03288
A_s	Min	0.1452		−0.189
	Max	0.1452	0.001452	−1.280
	Typical	0.1452		0.5570
ε_{eff}	Min	1.08		−0.378
	Max	1.08	0.054	−0.320
	Typical	1.08		−0.3334
T_w	Min	61.54		−0.263
	Max	26.87	0.5	10.28
	Typical	35.00		−1.974
T_g	Min	18.8		0.136
	Max	20.6	0.3	6.148
	Typical	20.5		1.164
Computed values		h		
	Min	7.895		
	Max	120.37		
	Typical	47.07		
Uncertainty, $\frac{\delta h}{h}$		Root sum square (%)		Worst-case (%)
	Min	6.78		14.91
	Max	10.04		16.17
	Typical	5.14		9.88

centered finite volume, pressure-corrector algorithm, was used in a steady formulation in all cases. Second order discretization was used for all variables and the density formulation used was incompressible-ideal-gas. This implies that the density of the flow varies with local gas temperature but not pressure. It was found that the momentum equation had to be significantly underrelaxed to achieve convergence and an underrelaxation factor of 0.3 was used.

2.2 Computational Domain and Boundary Conditions. A single blade was simulated using periodic boundary conditions. Considerable care had been taken with the experimental work to ensure that a periodic pressure distribution had been obtained around the aerofoil, particularly in the tip region, which allowed this approach to be used. This enabled a much smaller computational volume to be used, reducing the mesh sizes and allowing greater grid refinement. The computational domain used is shown in Fig. 3.

The inlet boundary layer was measured experimentally by the traverse of a total pressure probe at a maximum resolution of 1.27 mm on a plane 1.11 m upstream of the blade leading edge. The inlet turbulent intensity was also measured on this same plane using a hot-wire probe. In order to obtain appropriate boundary conditions for use with the periodic flow assumption, a computational fluid dynamics (CFD) simulation of the full three-passage cascade using the experimentally measured inlet conditions was

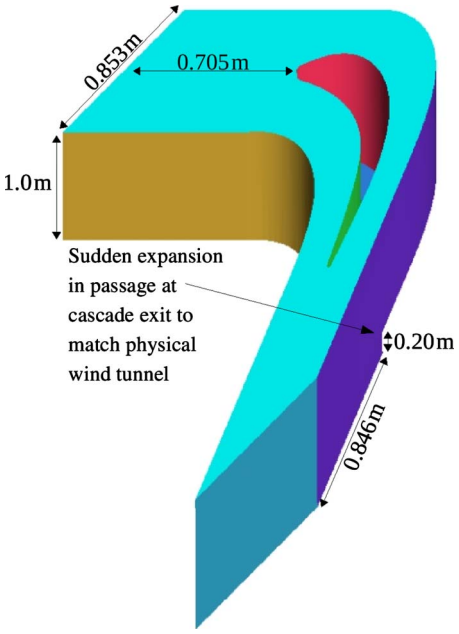

Fig. 3 Computational domain

performed and the flow conditions at the new inlet plane saved as a profile. This ensured representative inlet conditions were used in the final simulations.

To simulate the experiments, the CFD simulations were run with a constant heat flux boundary condition on the blade tip surface. The predicted blade tip surface temperature fields were then used to calculate the heat transfer coefficient and hence the Nusselt number fields.

2.3 Meshing Strategy. All meshes used were generated in ICEM CFD 11. A structured multiblock hexahedral approach was taken to allow the alignment of gridlines with the flow directions in order to aid convergence. A detail of the computational mesh in the region of the blade tip is shown in Fig. 4. Great care was taken to ensure good mesh quality throughout the domain, with both an inner O-grid (which lies in the tip gap above the solid blade) and an outer O-grid (which surrounds the blade) added around the aerofoil profile to keep cell skewness to a minimum. Cell growth ratios were kept below 1.2 and sudden changes in cell size between adjacent blocks were eliminated. For the coarse mesh intended for use with standard wall functions, the mesh sizing was chosen such that wall-adjacent cell y^+ values, as reported from *that* simulation, on the blade tip fell between 30 and 60, ensuring that the first cell was placed within the fully turbulent region of the boundary layer. By contrast, for the finer meshes where boundary layer resolution was attempted, wall-adjacent cell y^+

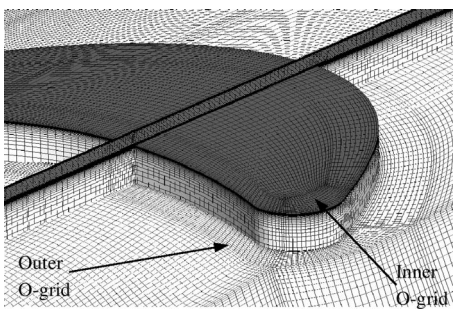

Fig. 4 Detail of blade tip mesh with mesh cut-planes ("fine (adjusted)" mesh shown)

Table 3 Summary of turbulence models

Turbulence model	
Spalart–Allmaras	Enhanced wall treatment used with fine meshes/standard wall functions used with coarse mesh
Standard k-ε	
Realizable k-ε	
RNG k-ε	
Standard k-ω	
SST k-ω	
Reynolds stress model	

values below 5 were achieved on the blade tip surface to ensure that the first node was placed within the laminar sublayer. This allowed the resolution of the boundary layer and thus avoids the need for wall functions based on an assumed boundary layer profile.

2.4 Moving Endwall. In order to test the effect of the moving endwall on the computational predictions, two simulations were run, one with the endwall stationary and one with the endwall moving at the engine representative speed of 4.7 m/s, using otherwise identical conditions.

2.5 Turbulence Models. All turbulence models available from the graphical user interface in FLUENT were tested, as detailed in Table 3. Where a near-wall treatment was required, the enhanced wall treatment was selected for use with the fine meshes (as detailed in Sec. 2.6), which blends a turbulence model valid in the viscous affected region with the selected turbulence model to allow resolution of the boundary layer. Standard wall functions were used with the coarse mesh.

Table 4 Summary of meshes

	Very fine	Fine	Fine (adjusted)	Coarse
Mesh size ($\times 10^6$)	5.0	2.8	2.8	0.5
Nodes in tip gap	40	33	37	8
First cell height in tip gap (mm)	0.05	0.1	0.1	3.8
Maximum cell height in tip gap (mm)	0.94	0.93	0.63	3.8
Maximum y^+ on blade tip (as reported from output)	1.1	2.0	2.0	60

2.6 Grid Independence Testing. In order to ensure grid independence, three meshes of varying refinements were created from the same blocking structure. These were relatively fine meshes designed to resolve the boundary layers. By comparing results from the very fine mesh with the fine mesh, the effect of the first cell height in the tip gap could be observed, while differences between the fine and fine (adjusted) meshes showed the impact of the maximum cell height within the tip gap. The meshes are summarized in Table 4 and illustrated in Fig. 5 for the tip gap region. All three meshes were run using the Spalart–Allmaras turbulence model and identical solver settings. These produced near identical Nusselt number distributions, leading to the conclusion that the simulations were indeed grid independent.

A fourth mesh, intended for use with standard wall functions, was also generated using the same blocking structure. This coarse mesh was designed to give a reported y^+ of between 30 and 60 over the blade tip surface, and as such is much coarser than the other meshes.

2.7 Convergence Criteria. Convergence of the simulations was judged on residual histories, mass flux imbalance, and the Nusselt number distribution on the blade tip. At convergence, all simulations had an overall mass flux imbalance of less than 0.5% and steady scaled residuals of below 10^{-3} (10^{-6} in the case of the energy residual). Furthermore, the simulation was run until the integral of the Nusselt number over the blade tip surface was unchanging with further iterations, ensuring that the Nusselt number distribution was steady.

3 Results

3.1 Flow Field. Pathlines from a simulation using the very fine mesh and the Spalart–Allmaras turbulence model are shown in Fig. 6. All of the flow features documented in the numerous flat-tip studies available in literature are visible. The leakage flow separates over the sharp pressure side edge, creating a captured vortex within the separation bubble. The over-tip leakage flow is approximately chordwise in the forward part of the blade tip and approximately perpendicular to the blade chord in the latter part. This leakage flow rolls up into a tip leakage vortex on meeting the main passage flow. This vortex counterrotates relative to the horseshoe passage vortex.

Figure 7 shows a comparison of flow velocity between the experimental data and simulations run on the very fine mesh and the coarse mesh in the crucial tip-gap region. Both simulations used

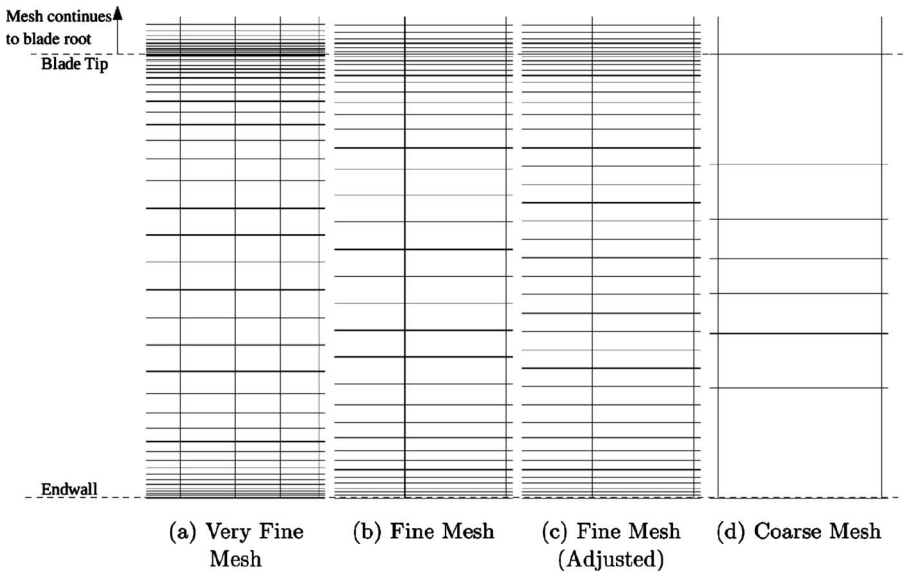

Fig. 5 Tip gap mesh refinement comparison

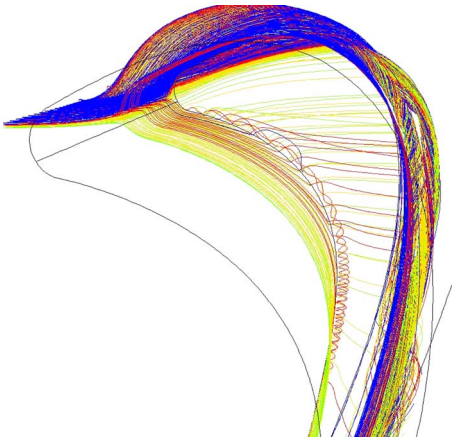

Fig. 6 Pathlines of flow over blade tip

the Spalart–Allmaras turbulence model. While there is some discrepancy in the magnitude of the flow velocities, the very fine mesh has correctly predicted the shape of the flow in the region, including the separation bubble underneath the pressure side edge. The location of flow reattachment on the tip surface is also correctly resolved. The results from just one of the fine meshes are presented here as the results from the three fine meshes are indistinguishable by the eye. By contrast, however, the coarse mesh lacks the resolution to predict adequately the over-tip leakage flow, with the simulated flow field bearing little resemblance to that which is measured. The separation bubble seen over the pressure side edge is entirely absent from the flow.

3.2 Heat Transfer Results. All heat transfer results are presented in the form of Nusselt number, which is defined as

$$\mathrm{Nu} = \frac{hC_{\mathrm{ax}}}{k} \tag{2}$$

where

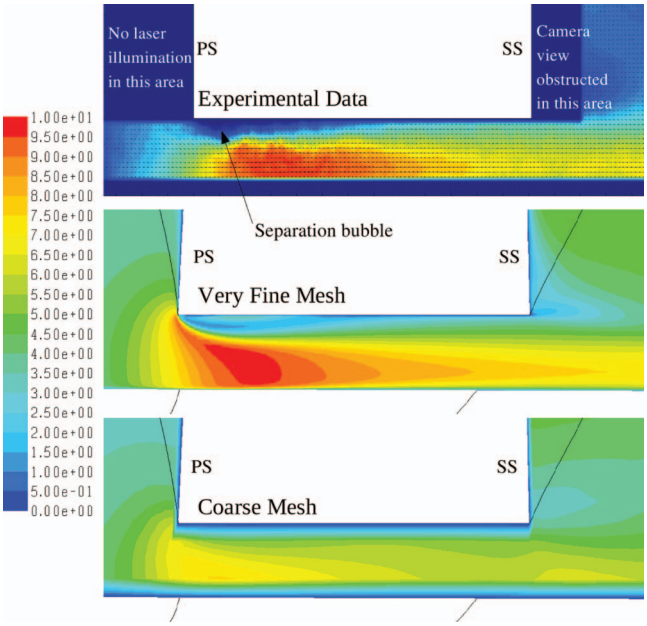

Fig. 7 Velocity (m s^{-1}) contours through the tip gap on a transverse plane

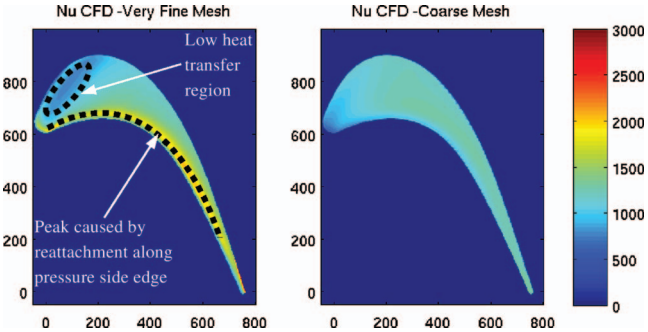

Fig. 8 Effect of grid size on Nusselt number distributions

$$h = \frac{q_{\mathrm{tip}}}{T_w - T_g} \tag{3}$$

This form directly scales local heat flux if small changes in total temperature caused by work done by the moving endwall may be ignored.

Figure 8 shows a comparison between the local Nusselt number distributions from the very fine mesh and the coarse mesh. The results from the very fine mesh have the expected shape of the heat transfer distribution, showing the peak near the pressure side from flow reattachment and the broad region of low Nusselt number found at the nose of the blade tip (the "sweet spot"). Once again, results from only a single fine mesh are presented, as the differences between the fine mesh results are barely discernible by the eye. However, the coarse mesh fails entirely to capture any of the key features in the heat transfer distribution. This is due to the lack of resolution preventing the correct flow field from being established, as already illustrated in Fig. 7. At high speed, the boundary layers would be thinner and a larger number of nodes would have to be present in the tip gap to achieve the same reported y^+ values. It is therefore unclear whether standard wall functions could be used for high speed environments. The highly disturbed nature of the flow field for more realistic, nonflat tips also suggests that the use of wall functions would not easily be justified. It should be noted that as the velocity field is incorrect, the reported y^+ values of 30–60 over the blade tip are not true y^+ values, as an incorrect value for u^* will have been calculated by the solver based on the computed flow field. However, this result is illustrative of the potential danger that could befall a CFD practitioner if appropriate checks are not made.

The heat transfer results from the moving endwall simulations are presented in Fig. 9. These runs used the very fine mesh and the Spalart–Allmaras turbulence model. The effect of the relative endwall motion is twofold. First, the peak in the heat transfer coefficient at the point of flow reattachment along the pressure side edge is slightly increased in magnitude, and second, the peak is shifted closer to the pressure side edge. These qualitative observations match those found in the experimental results.

The blade tip heat transfer results from the simulations using different turbulence models are plotted in Fig. 10, along with the experimental data. It should be noted that experimental data are not available right up to the edge of the tip, as the surface was viewed from inside the blade. The "rim" seen around the data does not, therefore, indicate any external physical feature. For these turbulence model tests, the fine (adjusted) mesh was used and the endwall was stationary. For ease of comparison, the percentage difference in Nusselt number between the experimental and numerical simulation data is shown in Fig. 11.

All of the turbulence models captured the qualitative trends of the Nusselt number distributions. Most of the turbulence models underpredicted the average heat transfer by around 35% compared with the experimental results. However, there are two notable exceptions—first, the standard k-ε model (with enhanced wall

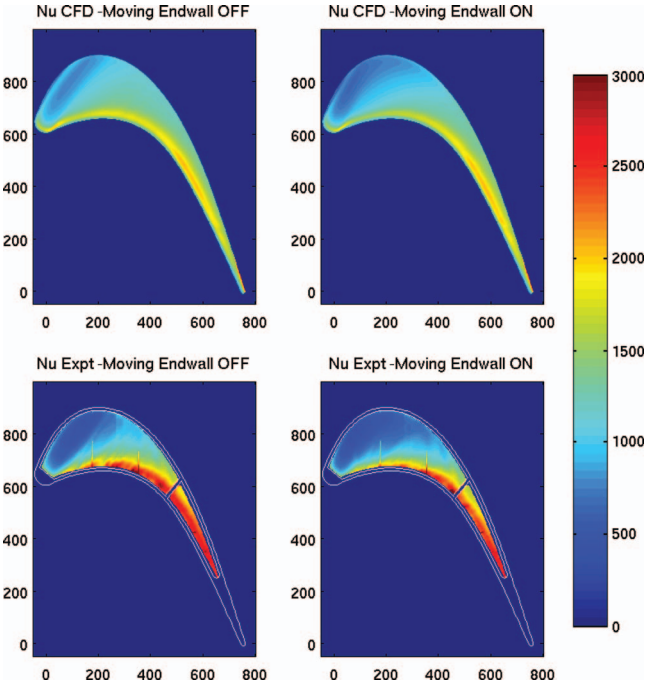

Fig. 9 Nusselt number distributions showing the effect of the moving endwall

treatment), which underpredicted Nusselt numbers by 20%, and second, the standard k-ω model, which agreed to within 5% of the measured values over the entire blade tip, except in the low heat transfer region. These two solutions, while achieving much closer Nusselt number magnitudes than the other turbulence models, both underpredicted the size of the separation region over the pressure side edge, placing the peak in heat transfer too close to the edge. These effects appear to be linked to a higher predicted turbulent viscosity and turbulent kinetic energy production in the pressure side tip region with the standard k-ε and standard k-ω models, both of which predicted turbulent viscosities an order of magnitude greater than the other turbulence models, as illustrated in Fig. 12. Interestingly, this may also account for the underpredicted extent of the separated flow in this region.

The relative performance of the turbulence models is quantified in Fig. 13. Here, the average mean absolute error in Nusselt number over the region where experimental data were collected is plotted. It should be noted that although the conclusions from the present study with regard to the accuracy of the different turbulence models appears to contradict those of the similar study by Yang et al. [11], the relative magnitudes of heat transfer predicted by the standard k-ε, the RNG k-ε, and the Reynolds stress model are the same (standard k-ε predicted the highest heat transfer coefficients, RSM the lowest). The inconsistency, therefore, lies not in the simulations themselves, but rather in how the experimental data compare with the computational results in the two studies.

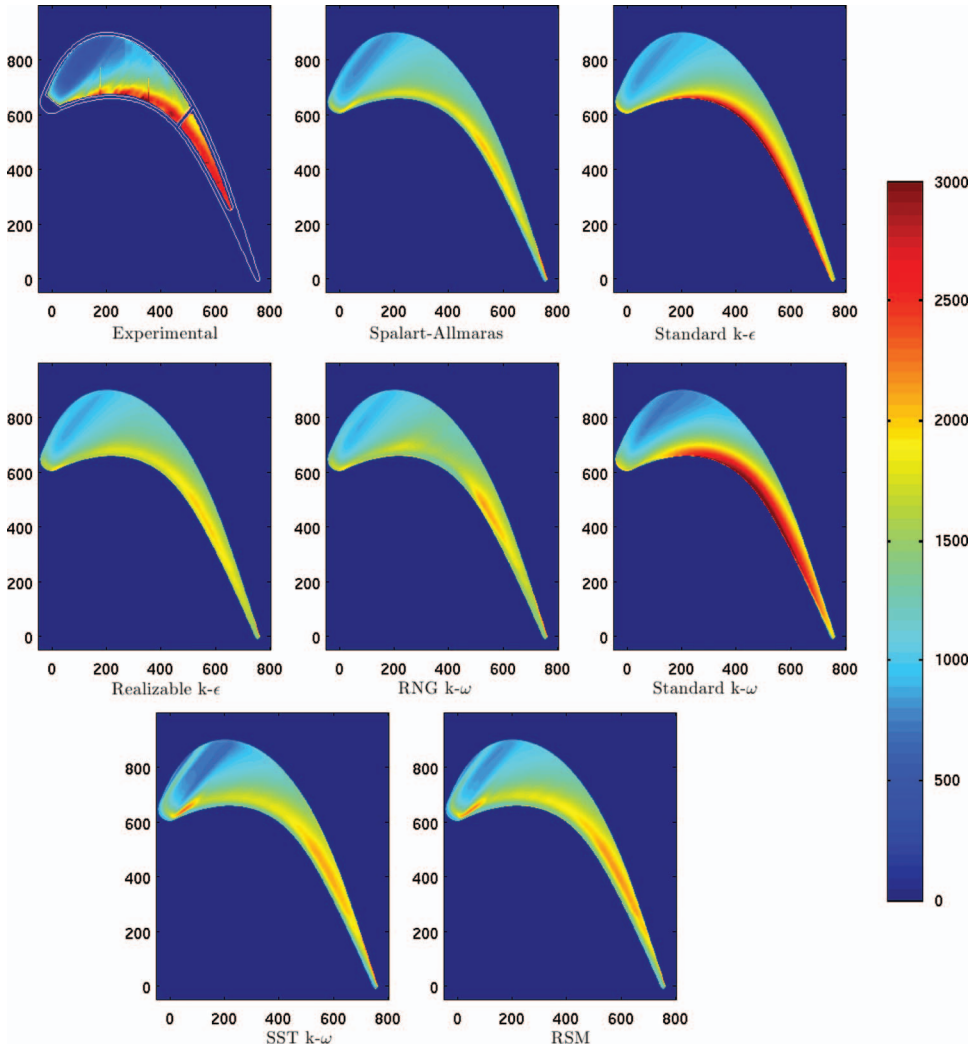

Fig. 10 Comparison of predicted blade tip Nusselt number distributions using different turbulence models with the experimental data

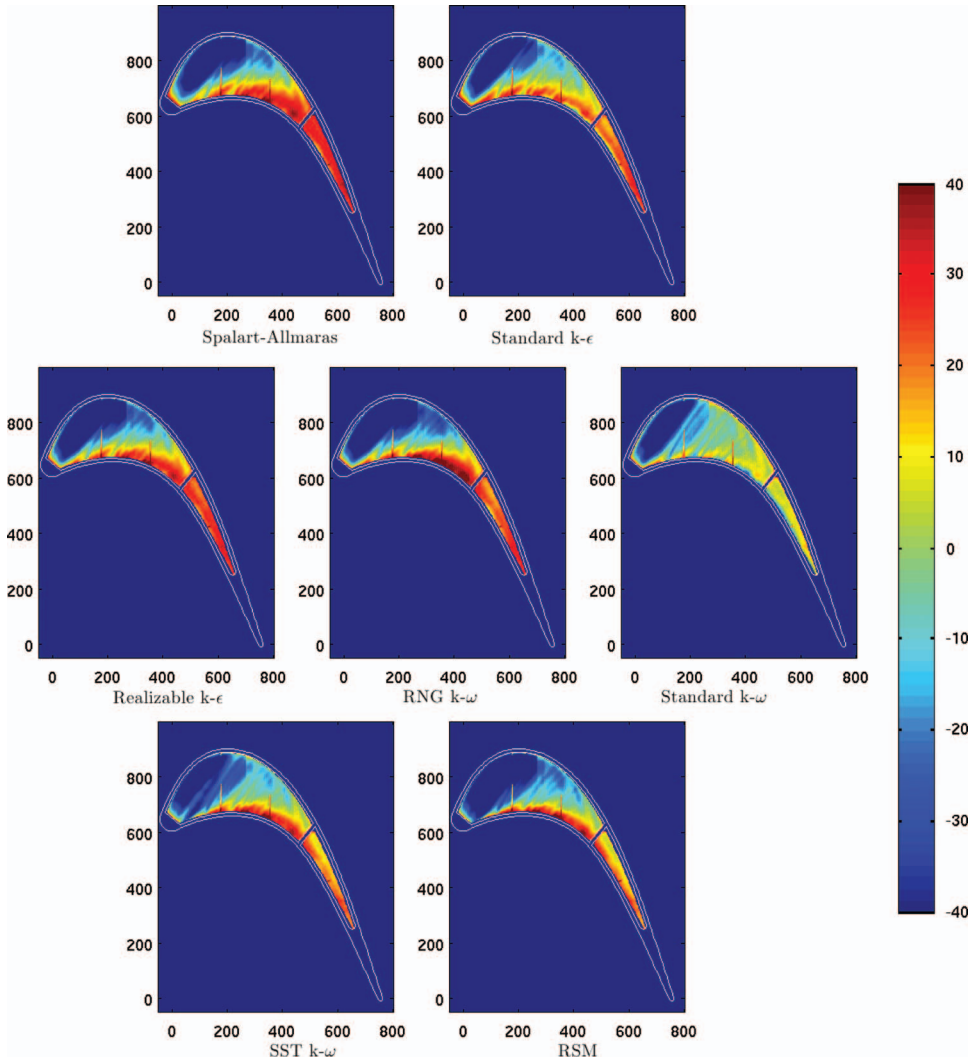

Fig. 11 Percentage difference between predicted and experimentally measured blade tip Nusselt number distributions using different turbulence models

4 Summary and Conclusions

In this paper, the computational simulation of blade tip heat transfer on an unshrouded, flat tip turbine blade in a linear cascade was performed using multiblock hexahedral meshes in FLUENT 6.3. The blade profile used is representative of a HP turbine blade from a modern aeroengine. Grid independence was tested and confirmed by the use of three meshes of varying refinements. The effect of the turbulence model on the heat transfer predictions was investigated by a thorough test of seven different models, and the veracity of the prediction assessed by comparison against experimental heat transfer data collected using the Oxford superscale cascade.

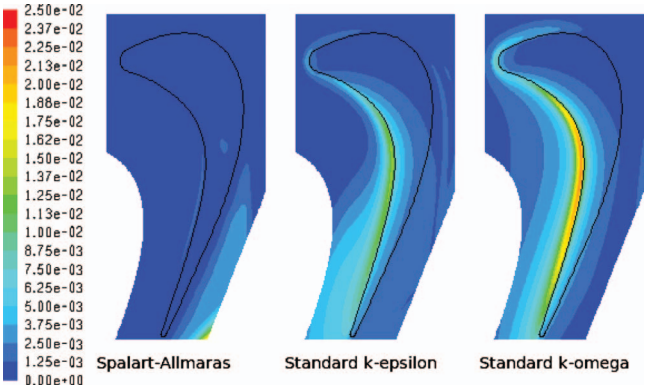

Fig. 12 Turbulent viscosity (Pa s) at the tip gap midplane

All of the expected flow features were correctly predicted, including the passage vortex, tip leakage vortex, and pressure side tip separation bubble. The simulations run with a moving endwall captured the effects observed experimentally with the moving belt; namely, an increase in the peak local Nusselt number and a reduction in size of the pressure side separation.

All seven turbulence models tested gave the correct qualitative distribution. Of these, the standard k-ω model performed the best, with a discrepancy in Nusselt number of just 5%, followed by the standard k-ε model, with a 20% error. The other models tested were very similar and gave errors of around 35%.

It is recommended that investigators computing similar flow fields try the standard k-ω model first before comparing the predictions with those given by other models. Those with, for example, squealer tips are advised to consult Ref. [12] before proceeding, as the conclusions reached here may not necessarily apply.

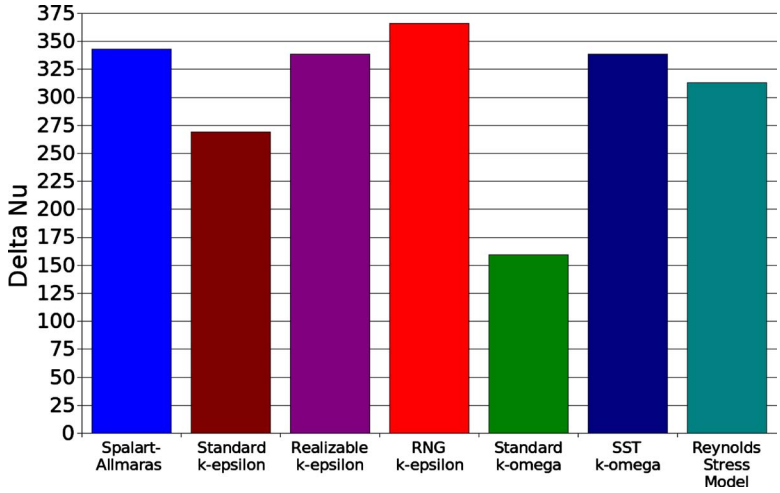

Fig. 13 Mean absolute error in Nu

Acknowledgment

This work was sponsored by Rolls-Royce plc, and the authors would like to thank them for their support.

Nomenclature

A_s = tip surface area, m^2
C_{ax} = axial chord, m
ε = emissivity
ε_{eff} = effective emissivity
h = heat transfer coefficient, $W\ m^{-2}\ K^{-1}$
I = heater supply current, A
k = thermal conductivity, $W\ m^{-1}\ K^{-1}$
μ = dynamic viscosity, Pa s
Nu = Nusselt number $(=hC_{ax}/k)$
q_{tip} = heat flux through the tip surface, $W\ m^{-2}$
R = heater resistance, Ω
Re = Reynolds number $(=\rho\nu_{ex}C_{ax}/\mu)$
σ = Stefan–Boltzmann constant $(=5.670\times10^{8}\ W\ m^{-2}\ K^{-4})$
T_w = local wall temperature, °C
T_g = upstream gas temperature, °C
τ_w = wall shear stress, $N\ m^{-2}$
u^* = friction velocity $(=\sqrt{\tau_w/\rho})$, $m\ s^{-1}$
V = heater supply voltage, V
v_{ex} = cascade exit velocity, $m\ s^{-1}$
y = distance to the wall, m
y^+ = nondimensional distance to the wall $(=\rho y u^*/\mu)$

References

[1] Bunker, R. S., 2001, "A Review of Turbine Blade Tip Heat Transfer," Ann. N.Y. Acad. Sci., **934**(1), pp. 64–79.
[2] Mayle, R. E., and Metzger, D. E., 1982, "Heat Transfer at the Tip of an Unshrouded Turbine Blade," *Heat Transfer 1982—Proceedings of the Seventh International Heat Transfer Conference*, München, Federal Republic of Germany, Sept. 6–10, U. Grigull, E. Hahne, K. Stephan, and J. Straub, eds., Vol. 3, pp. 87–92.
[3] Yaras, M. I., and Sjolander, S. A., 1992, "Effects of Simulated Rotation on Tip Leakage in a Planar Cascade of Turbine Blades: Part I—Tip Gap Flow," ASME J. Turbomach., **114**(3), pp. 652–659.
[4] Azad, Gm. S., Han, J. C., Teng, S., and Boyle, R. J., 2000, "Heat Transfer and Pressure Distributions on a Gas Turbine Blade Tip," ASME J. Turbomach., **122**(4), pp. 717–724.
[5] Azad, Gm. S., Han, J. C., and Boyle, R. J., 2000, "Heat Transfer and Flow on the Squealer Tip of a Gas Turbine Blade," ASME J. Turbomach., **122**(4), pp. 725–732.
[6] Kwak, J. S., Ahn, J., Han, J. C., Lee, C. P., Bunker, R. S., Boyle, R., and Gaugler, R., 2003, "Heat Transfer Coefficients on the Squealer Tip and Near-Tip Regions of a Gas Turbine Blade With Single or Double Squealer," ASME Paper No. GT2003-38907.
[7] Bunker, R. S., Bailey, J. C., and Ameri, A. A., 2000, "Heat Transfer and Flow on the First-Stage Blade Tip of a Power Generation Gas Turbine: Part 1—Experimental Results," ASME J. Turbomach., **122**(2), pp. 263–271.
[8] Ameri, A. A., and Bunker, R. S., 2000, "Heat Transfer and Flow on the First-Stage Blade Tip of a Power Generation Gas Turbine: Part 1—Simulation Results," ASME J. Turbomach., **122**(2), pp. 272–277.
[9] Wilcox, D. C., 1994, "Simulation of Transition With a Two-Equation Turbulence Model," AIAA J., **32**(2), pp. 247–255.
[10] Menter, F. R., 1993, "Zonal Two-Equation k-ω Turbulence Models for Aerodynamic Flows," 24th Fluid Dynamics, Plasmadynamics, and Lasers Conference, Orlando, FL, Jul. 6–9, Paper No. AIAA-93-2906.
[11] Yang, H., Acharya, S., Ekkad, S. V., Prakash, C., and Bunker, R., 2002, "Flow and Heat Transfer Predictions for a Flat-Tip Turbine Blade," ASME Paper No. GT2002-30190.
[12] Yang, H., Acharya, S., Ekkad, S. V., Prakash, C., and Bunker, R., 2002, "Numerical Simulation of Flow and Heat Transfer Past a Turbine Blade With a Squealer-Tip," ASME Paper No. GT2002-30193.
[13] Palafox, P., 2006, "Gas Turbine Tip Leakage Flow and Heat Transfer," DPhil thesis, Oxford University, Oxford, UK.
[14] Palafox, P., Oldfield, M. L. G., LaGraff, J. E., and Jones, T. V., 2008, "PIV Maps of Tip Leakage and Secondary Flow Fields on a Low-Speed Turbine Blade Cascade With Moving End Wall," ASME J. Turbomach., **130**(1), p. 011001.
[15] Palafox, P., Oldfield, M. L. G., Ireland, P. T., Jones, T. V., and Lagraff, J. E., 2006, "Blade Tip Heat Transfer and Aerodynamics in a Large Scale Turbine Cascade With Moving Endwall," ASME Paper No. GT2006-90425.
[16] Moffatt, R. J., 1982, "Contributions to the Theory of Single-Sample Uncertainty Analysis," ASME J. Fluids Eng., **104**, pp. 250–260.